

Earth Observation and Geomatics Engineering

Online ISSN: 2588-4360

Homepage: https://eoge.ut.ac.ir/

3D Reconstruction Accuracy Assessment of UAV-based Photogrammetry Products: Modeling of GCPs Pattern, Number, and Spatial Distribution

Mortaza Dorzadeh ¹ , Hassan Emami ² □

- 1. Department of Geomatics, University of Tabriz, Tabriz, Iran. E-mail: mortezaa.dorzadeh@gmail.com
- 2. Corresponding author, Department of Geomatics, University of Tabriz, Tabriz, Iran. E-mail: h_emami@tabrizu.ac.ir

Article Info

Article type:

Research Article

Article history:

Received 2025-04-19 Received in revised form 2025-05-24 Accepted 2025-06-08 Published online 2025-10-19

Keywords:

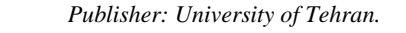
UAV-based, photogrammetry, 3D Reconstruction, GCPs Network, Structure from motion

ABSTRACT

The objective of this research is to examine and model the influence of ground control point (GCP) configurations, quantity, spacing, and spatial distribution on the accuracy of 3D reconstruction in UAV-based photogrammetry. Four GCP patterns were evaluated: Mode A (minimal corner placement), Mode B (perimeter distribution), Mode C (combined perimeter and central), and Mode D (central-only), across three scenarios with increasing GCP spacing in urban and non-urban areas. The total GCPs ranged from 4 to 42, with distances tested at 100m (1D), 200m (2D), and 300m (3D), corresponding to multiples of 30, 60, and 90 times the GSD. Local accuracy was assessed using 30 random checkpoints, while global accuracy was analyzed via the M3C2 algorithm. Scenario 1 (1D spacing) revealed Mode B achieved the highest local accuracy, with RMSE values of 0.10 m (urban) and 1.06 m (non-urban). Scenario 2 (2D spacing) showed slight accuracy reductions but maintained comparable performance. In Scenario 3 (3D spacing), Mode C outperformed others, yielding an RMSE of 0.17 m (urban) and 0.80 m (non-urban), with errors concentrated at block edges. Global M3C2 analysis confirmed Mode C's superiority in Scenario 3, demonstrating that central GCP placement becomes critical when spacing exceeds 90×GSD. Results indicate that perimeterbased configurations (Mode B) suffice for smaller intervals ($\leq 30 \times GSD$), but larger spacings (>90×GSD) necessitate combined perimeter and central GCPs (Mode C) to mitigate accuracy degradation. Mode C is recommended for large-scale projects with sparse GCP networks, balancing efficiency and reliability.

Cite this article: Dorzadeh, M., & Emami, H. (2025). 3D Reconstruction Accuracy Assessment of UAV-based Photogrammetry Products: Modeling of GCPs Pattern, Number, and Spatial Distribution, Earth Observation and Geomatics Engineering, Volume8 (Issue2), Pages 34-50. http://doi.org/10.22059/eoge.2025.392733.1175.

© The Author(s).





DOI: http://doi.org/10.22059/eoge.2025.392733.1175

1. Introduction

Various photogrammetry and computer vision algorithms based on dense corresponding point matching approaches have been developed to analyze images and perform automated 3D reconstruction. Unmanned Aerial Vehicles (UAVs) have emerged as a pivotal tool for data acquisition, driving innovations across geosciences, remote sensing, and precision mapping (Nex et al., 2022). The integration of lowcost sensors with UAV platforms (Koeva, Muneza, Gevaert, Gerke, & Nex, 2018) has further expanded 3D mapping applications in agriculture, urban planning, environmental monitoring, and disaster management (Jenal et al., 2020; Yin et al., 2023). UAVs are broadly categorized into military, reconnaissance, civilian, and logistics drones, with their photogrammetric capabilities increasingly leveraged for high-resolution spatial analysis (Fernandez Galarreta, Kerle, & Gerke, 2015). Studies highlight the efficacy of UAV-based photogrammetry in diverse scenarios. For instance, Peppa, Mills, Moore, Miller, and Chambers (2019) demonstrated centimeter-level accuracy in landslide monitoring using UAV-derived data and ground control points (GCPs). Similarly, Clapuyt, Vanacker, and Van Oost (2016) emphasized the critical role of GCP distribution in enhancing 3D topographic reconstruction precision via Structure-from-Motion (SfM)algorithms. Erenoglu, and Arslan (2018) underscored the potential of UAV-generated 3D models for urban planning, noting that accuracy depends on factors like camera specifications, image resolution, and area coverage. Collectively, these advancements underscore UAV photogrammetry as a versatile, cost-effective solution for high-precision 3D modeling, though challenges related to sensor limitations and environmental variability persist.

The number, spatial distribution, and network structure of Ground Control Points (GCPs) significantly influence the accuracy of UAV-based photogrammetric outputs. Varbla, Puust, and Ellmann (2021) demonstrated that UAVs equipped with RTK-GNSS require only a few GCPs to achieve geometric accuracy exceeding 5 cm. Elkhrachy (2021) reported horizontal and vertical RMSEs of 4-6 cm and 5-6 cm, respectively, using 21 GCPs, with errors correlating to ground sampling distance (GSD). Liu et al. (2022) emphasized that increasing GCP numbers reduces RMSE until a threshold density is reached, stressing the need for uniform distribution, including central placement. James, Robson, d'Oleire-Oltmanns, and Niethammer (2017) identified GCP measurement errors as critical factors affecting DEM accuracy through Monte Carlo simulations. Agüera-Vega, Carvajal-Ramírez, and Martínez-Carricondo (2017) found optimal horizontal and vertical accuracy with 15-20 GCPs, while Nagendran, Tung, and Ismail (2018)

confirmed centimeter-level accuracy necessitates GCPs across varying UAV altitudes. Martínez-Carricondo et al. (2018) recommended perimeter and interior GCP placement at 0.5-1 GCP/ha. Villanueva, Blanco, and Sciences (2019) linked DEM accuracy to uniform GCP distribution, and Awasthi et al. (2019) highlighted distribution patterns' impact on corridor mapping. Stöcker, Nex, Koeva, and Gerke (2020) underscored the combined influence of flight configuration, land cover, and GCP setup on data quality. Lalak, Wierzbicki, and Kędzierski (2020) proposed optimized GCP usage for single-strip adjustments. Oniga, Breaban, Pfeifer, and Chirila (2020) observed diminishing returns beyond 20 GCPs, achieving a 50% RMSE reduction. Long et al. (2021) determined five GCPs suffice for <10 cm accuracy in 36-ha mines. Zhang et al. (2022) advocated two-dimensional GCP distributions over linear arrangements. Carvajal-Ramírez, Agüera-Vega, and Martínez-Carricondo (2016) achieved sub-0.1 m accuracy with edge-distributed. Reshetyuk and Mårtensson (2016) recommended 1.8 GCPs/ha for precision. Gindraux (2019) generalized optimal GCP distribution principles, while Sanz-Ablanedo, Chandler, Rodríguez-Pérez, and Ordóñez (2018) suggested ≥3 GCPs/100 images for large-scale projects, translating to ~2590 ha (3581 images) for their study. Collectively, these studies highlight the necessity of balancing GCP quantity, density (often 0.5-2 GCPs/ha), and spatial uniformity to maximize photogrammetric accuracy across diverse applications.

Previous studies have explored the influence of control points and their distribution to some extent, each with a distinct aim and application. However, no unique model has been developed, nor has a full evaluation of the geographical distribution, quantity, and configuration of GCPs in different UAV geomatics projects been conducted. A previous study demonstrated that a variety of factors affect the accuracy of UAV photogrammetry outputs. While thoroughly investigating the spatial distribution pattern of GCPs, as well as their quantity and suitable distance, the following two key aims are pursued: The primary objective of this study is to assess the impact of GCP's network configuration pattern, number, and spatial distribution on UAV-based photogrammetry and 3D reconstruction accuracy. The second objective is to determine the optimal distances between the GCPs in order to improve the accuracy of the orthomosaic acquired by UAV photogrammetry.

2. Material and method

2.1 Study area and dataset

This investigation was conducted at Tafarsh University in a region related to Iran, with latitude (50° 47′ 02 to 50° 30′

03) and longitude (50° 22' 40 to 57° 40" 50°). A drone was utilized to image the university's main and surrounding campuses, which cover an area of 120 meters above the surface and 0.297 square kilometers. This area has distinctive aspects of many landscapes, such as roads and buildings, and is barren yet distinct in terms of topographic variation. The data was collected on July 27, 2019. Figure 1 shows the study area.

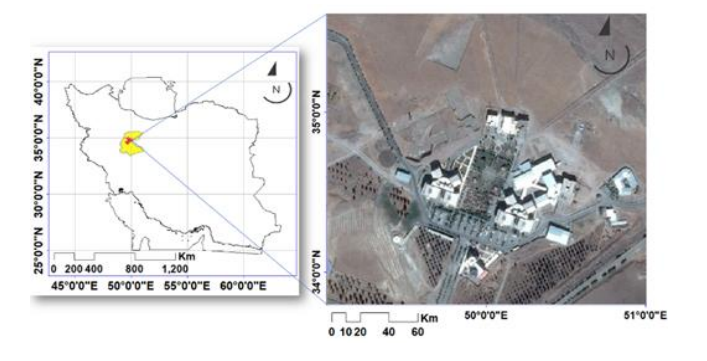


Figure 1. The area studied in this research

Before beginning the imaging of the research region, an appropriate flight plan with several factors such as flying height, GSD, and total number of images was established. Using equation 1, a suitable value of GSD, which impacts the quality of the final findings and the details of the orthomosaic, was found for a certain flight height H (Tu et al., 2020). To that end, the DJI Phantom 4 Pro (a DJI Pro Platinum drone equipped with an RGB camera (FC6310s)) was used to capture images on July 27, 2019. Lens length was 8.8 mm, ISO was 100, shutter speed was 800 1/second, sensor width was 13.2 mm, sensor length was 8 mm, and the image size was 5472 x 3648 pixels.

$$GSD = \frac{Sw \times H \times 100}{Fr \times Imw}$$
 (1)

Where Sw represents the real sensor width (mm), Fr corresponds to the real focal length (mm), and Imw represents the image width in pixels. A GSD of 3.29 cm/pixel, for example, can be reached with a DJI Pro drone at a flying height of 120 meters. GCPs were utilized to georeference the images acquired by the photogrammetry UAV. The GCP was obtained using the RTK GNSS method with centimetr horizontal and vertical accuracy. Figure 2 illustrates the GCPs utilized in this study.

This study demonstrates the structural influence of GCPs design, number, optimum distance, and spatial distribution pattern in determining the accuracy of the reconstruction of 3D models based on UAV photogrammetry. To end that, 194 UAV images were collected during the data collection stage,

and then a geodetic network of 42 GCPs was designed using the GNSS positioning system.

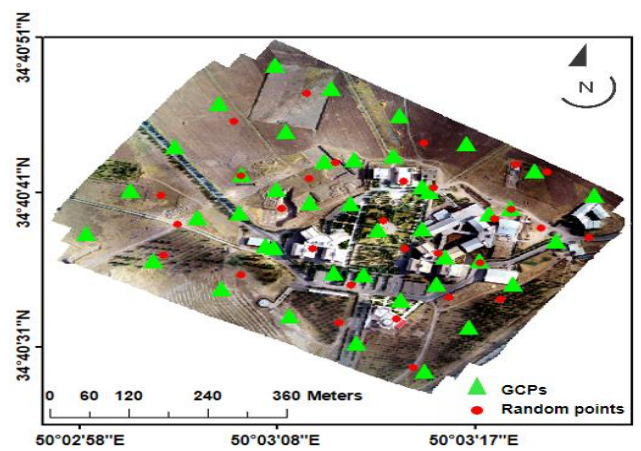


Figure 2. The GCP and random point's distribution.

2.2. Proposed method

According to the reviewed studies outlined in the Introduction, the optimal number of ground control points (GCPs) in UAV-based photogrammetry projects depends on multiple factors. Technical standards generally recommend a density of 1 to 5 GCPs per hectare, with higher densities (e.g., ~1 point per 0.5 ha) required for centimeter-level accuracy (±3 cm). In this 30-hectare project, 42 GCPs (1.4 points per hectare) reflect high precision demands or complex terrain conditions. These points may serve dual roles: a subset (e.g., 30 points) for the results were assessed locally processing and the remainder (e.g., 12 points) as checkpoints to validate final accuracy. Uniform spatial distribution is critical to minimize DEM and orthomosaic errors; in the 550 x 550 m study area, 42 points achieve a ~80-100 m spacing, ensuring balanced coverage. Four distribution patterns (A, B, C, and D) were evaluated to optimal configuration. identify Additionally, topographic complexity—such as steep slopes, vertical structures, or dense vegetation—necessitates more GCPs to address image distortions and enhance alignment. Ultimately, the selection of 42 points balances high accuracy requirements, complex terrain, and adherence to technical standards, ensuring sufficient spatial precision for mapping, environmental analysis, or land management applications.

It is a fact that the number of ground control points in drone-based photogrammetry projects increases proportionally to the area of the study area. Then, the mathematical model (2) can be written as

$$N_{GCP} \propto \sqrt{A} \rightarrow N_{GCP} = K_1 \sqrt{A} \cong K_1 \frac{\sqrt{A}}{GSD}$$
 (2)

Where N_{GCP} is the number of control points required and Where \sqrt{A} (length) divided by GSD (length) yields a dimensionless count, and K_1 (e.g., 2–3) is an empirical coefficient. In addition, the distance between ground control points depends on the GSD value and the expected final accuracy in the project under study. Therefore, the mathematical model (3) can be written as follows:

$$Dist_{GCP} \propto GSD \rightarrow Dist_{GCP} = K_2 \times GSD$$
 (3)

Where $Dist_{GCP}$ is the optimal distance between the required control points in meters, GSD is the ground sampling distance in meters, and K_2 is a constant coefficient that depends on the required accuracy of the research. Furthermore, the relationship between the accuracy of the project can be calculated by considering the GSD from the mathematical model (4):

$$\delta_{Proj} \propto GSD \rightarrow \delta_{Proj} = \frac{GSD}{Scale\ Factor}$$
 (4)

Where, δ_{Proj} is the average desired accuracy of the project (average vertical and planimetric accuracy), GSD is the ground sampling distance in meters, and the scale factor depends on the data coverage and the data abundance, considering the normal distribution and establishing a balance between accuracy and cost, between 2 and 3 can be considered.

Considering mathematical relations (1) to (4), in order to determine a more accurate mathematical model, the above relations should be combined with each other, and the project accuracy should be considered as a coefficient (δ) of GSD. The optimal number of desired control points can be obtained from the proposed mathematical model (5):

$$N_{GCP} = \left(\frac{K_2}{\delta \times GSD - K_1 \times GSD}\right)^2 \tag{5}$$

This proposed model shows that if the GSD decreases, i.e., the imaging quality increases, the number of required control point's decreases. In addition, for a fixed GSD, increasing the number of ground control points can reduce the absolute error of the project. Furthermore, as the GSD increases, that is, as the resolution of the images decreases, the number of ground control points required increases. This result is logical because the positioning accuracy decreases with increasing GSD, so to compensate for this decrease in accuracy, a larger number of ground control points are required. First, before beginning to capture the region under investigation, a suitable flight plan is created using Equation 1, taking into account elements such as flight altitude, ground sampling distance (GSD), image coverage,

and imaging camera specifications. In reality, GSD depends on other metrics and variables in a UAV-based photogrammetry project (Eq. (1)). Second, the planimetry and vertical accuracy of UAV-based photogrammetry projects are chosen in relation to GSD using Equation 4. In UAV-based photogrammetry, horizontal and vertical accuracy are proportional to GSD (ground sampling distance). Accuracy standards for digital geospatial data are based on the ASPRS (American Society for Photogrammetry and Remote Sensing) Positional Accuracy for Digital Geospatial Data Standards (https://www.asprs.org/asprs-publications) and empirical methods (Remondino, F., et al. (2011) and Žabota, B., & Kobal, M. (2021)). Planar accuracy is typically considered to be 1 to 3 times the numerical value of GSD. In addition, elevation accuracy is usually 2 to 5 times the numerical value of GSD. In this proposed model, it is assumed that the control points are distributed uniformly over the study area so that their distances can be determined by calculating the number of points in the entire area. To optimize the proposed model, we optimize the model coefficients using a least squares algorithm. This optimization can be adjusted for specific conditions of UAV-based projects, for example, for a specific sensor, or for a specific flight altitude, or based on a specific project accuracy, all of which are usually dependent on the GSD. In the present study, based on the project specifications, the values of K₁ and K₂ were determined to be 28.84 and 4.59, respectively. This study's proposed method consists of four major steps: planning (field survey, pre-flight, and flight line adjustment); data collection; planning and survey; and data analysis GCPs. Data processing with various approaches in consideration: bundle adjustment and intense image matching; and horizontal and vertical quality evaluation (data and error analysis). Figure 3 shows the process of this investigation.

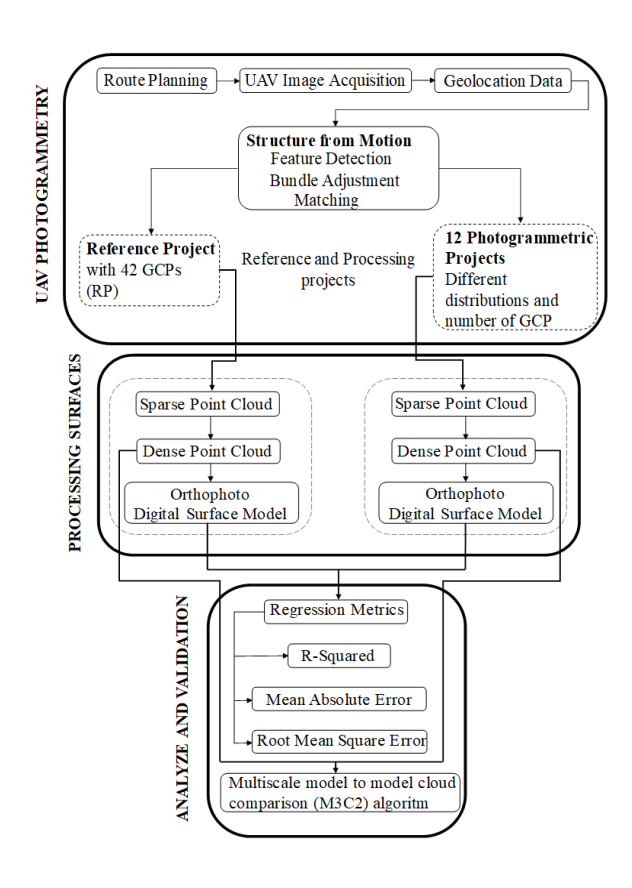


Figure 3. Research flowchart

The workflow in this study is such that after inputting the images into the Metashape Agisoft, the initial step of SfM, which involves image alignment and camera parameter viewing angle computation, is done. After that, a 3D point cloud was built. Based on this sparse point cloud, a highdensity point cloud was generated. The output of SfM was a DSM and orthomosaic based on the high-density point cloud. As a result, position calibration using a welldistributed collection of GCPs should be done immediately after the point cloud is produced to offer precise position information to these photogrammetry findings. Utilizing the obtained data, and after establishing and identifying the position of GCPs in each image, images were matched using the Agisoft software. The bundle adjustment method was employed, as was the simultaneous estimation of the interior and exterior orientation aspects of the images and the process of improving the camera orientation by optimizing the model based on the control points. After that, the initial parameters, as well as the most appropriate settings and variables, were then defined for all 42 GCP networks during

the data processing stage. Table 1 shows how to determine the initial parameters.

Table 1. Information about the UAV images and DEM processing.

parameter	Number	attributes	value
No. images	194	tie points	111,534
area	0.297 km ²	error	1.09 pix
Accuracy	Medium	RMSExy	0.78 m
G.Preselection	Enabled	RMSEz	0.96 m
R. Preselection	Yes	RMSExyz	1.25 m
Key.P. Limit	40, 000	points cloud	21,802,820
Tie.P.Limit	4, 000	Resolution	0.1 m

In this research, the output of this data set with 42 GCPs was employed as a processing reference, and the product of orthomosaic was regarded as a reference model. Figure 4 illustrates the orthomosaic product with 42 GCPs. The number, spatial distribution, and distances of these GCPs were changed in the calculations and examined in each subsequent processing stage while maintaining these initial parameters, and a method was presented to evaluate the effect of the spatial distribution, quantity, and optimal distance of GCPs on the quality of the results. The findings of the three primary characteristics of the number, spatial distribution, and distances of control points were assessed in each procedure to evaluate the accuracy of the UAV-based photogrammetric orthomosaic output.

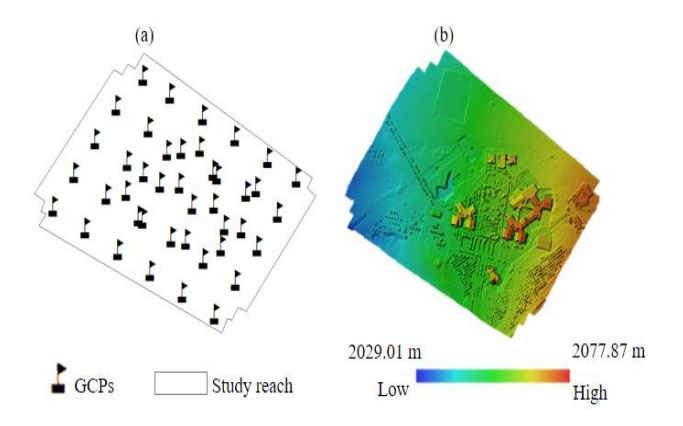


Figure 4. Orthomosaic result using all 42 GCPs as a reference model.

2.2.1 Distribution testing

Four alternatives—A, B, C, and D—with various control

point distribution patterns and configurations were evaluated to identify the optimum spatial distribution of GCPs. Mode A was used to design the minimum GCPs in the corners of the UAV photogrammetry block. Mode B was employed to design in all models around the photogrammetry block, and mode C was utilized to design GCPs around and in the middle of the photogrammetry block, and mode D was used to design only in the middle and center of the photogrammetry block.

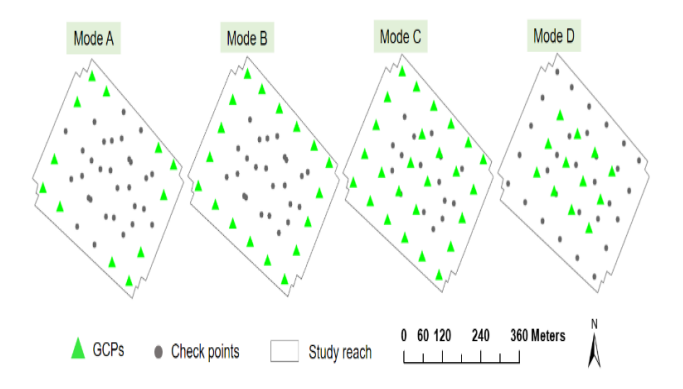


Figure 5. The various modes for testing the dispersion spatial distribution of GCPs to maximum distances of 1D = 30 GSD.

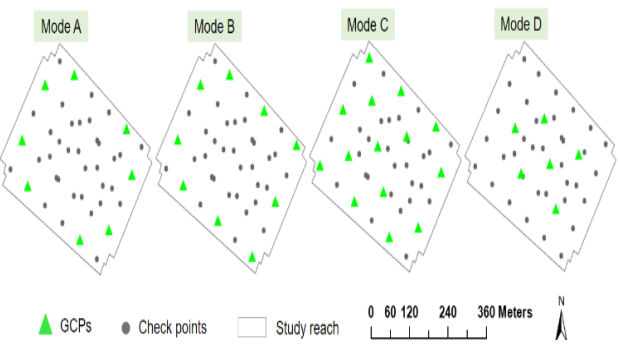


Figure 6. The various modes for testing the dispersion spatial distribution of GCPs to maximum distances of 2D

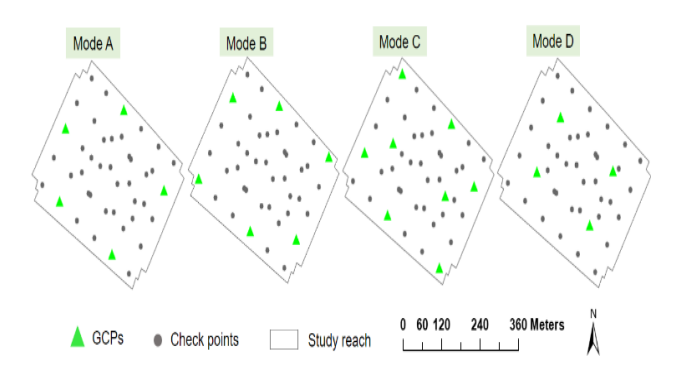


Figure 7. The various modes for testing the dispersion spatial distribution of GCPs to maximum 3D distances.

That is, depending on the distance between the GCPs, the total number of control points employed in all modes ranged from 4 to 42. In each of the four modes mentioned, a series of control points were used to construct an orthomosaic using the same initial parameters as the reference mode. The RMSE and the MAE were utilized as orthomosaic accuracy and quality metrics. Figures 5, 6, and 7 demonstrate the four modes A, B, C, and D of different spatial disturbances and checkpoints used in the construction and assessment of the UAV's photogrammetric orthomosaic result, respectively.

2.2.2 Distance testing

Based on the review studies in the introduction, optimal accuracy of elevation maps is achieved when we have one control point on average per hectare, i.e., 100 sauare meters. Accordingly, in this research, the distances between control points were considered as 100 meters and coefficients of that. In this research, the designations 1D, 2D, and 3D were used to denote the spacing between ground control points (GCPs) as multiples of the ground sampling distance (GSD: 30 cm). The first scenario (high-density GCPs) used the 1D configuration (equal to 100 meters (30 \times GSD) as the baseline for both urban and non-urban areas. The 2D (200 meters, $60 \times GSD$) and 3D (300 meters, $90 \times$ GSD) configurations were used in the second and third scenarios, respectively, doubling and tripling the GCP spacing relative to the first scenario to assess the impact of reduced GCP density on the accuracy of photogrammetric outputs, such as point clouds and orthomosaics. To investigate the optimal GCP distances, they were considered in such a way that the control points chosen for processing the photogrammetric processes of the UAV and its products had approximately 30 GSD = 100 m = 1D, 200m = 2D, and 300m = 3D. The objective of this experiment was to determine the extent to which the distance between the GCPs influences the accuracy of the base UAV's photogrammetric

output. As orthomosaic accuracy and quality measurements, the RMSE and the MAE were used.

2.2.3 Number of control point testing

The number of control points in the photogrammetric findings of the base UAV is investigated for error propagation. The number of control points is examined in distinct scenarios to determine the influence the number of GCPs has on the UAV's photogrammetric results. As a result, increasing the distance and lowering the number of GCPs are used to process each of the four configuration alternatives. That is, depending on the distance between the GCPs, the total number of control points employed in all modes ranged from 4 to 42. The findings were assessed locally using random points in the building and non-building regions, as well as globally using the multiscale model-to-model cloud comparison (M3C2) algorithm. Table 2 Show the summary of the different configurations and scenarios of this research.

Table 2. The summary of the different configurations and scenarios of this research

	Scenario	GCP	GCP	Environment
Mode	Securito	Distance	Placement	
A	1	1D	. Corner of area . focused	Non- urban/Urban
		(100m)		
	2	2D		
		(200m)		
	3	3D		
		(300m)		
В	1	1D	Perimeter	Non-
	2	2D	of area urban/Urban focused	
	3	3D		urban/Orban
	1	1D		
С	1	(100m)	Perimeter	
	2	2D	and center	Non-
		(200m)	hybrid	urban/Urban
	3	3D	пурна	
	3	(300m)		
D	1	1D	Central of	Non- urban/Urban
	2	2D	area	
	3	3D	focused	

3 Results and discussion

3.1 Comparison random points on point cloud

To evaluate the outcomes of four UAV photogrammetry modes (A, B, C, and D) based on the first, second, and third scenarios. The random point design was performed to first verify the errors locally and then analyze the local influence of the random points' proximity or distance to the GCPs on the point clouds produced by photogrammetry-based UAV outputs. We investigated 30 random points in two independent areas, one in construction areas and the other in non-construction areas, for this purpose. The building regions and randomly selected points were usually concentrated in the middle of the study area. The distance between the GCPs was considered to be around 1D in the first scenario in the non-urban region, and for four cases (A, B, C, and D), the examination results are outlined in Figures 8a, b, c, d, i, j, g, and 8 h.

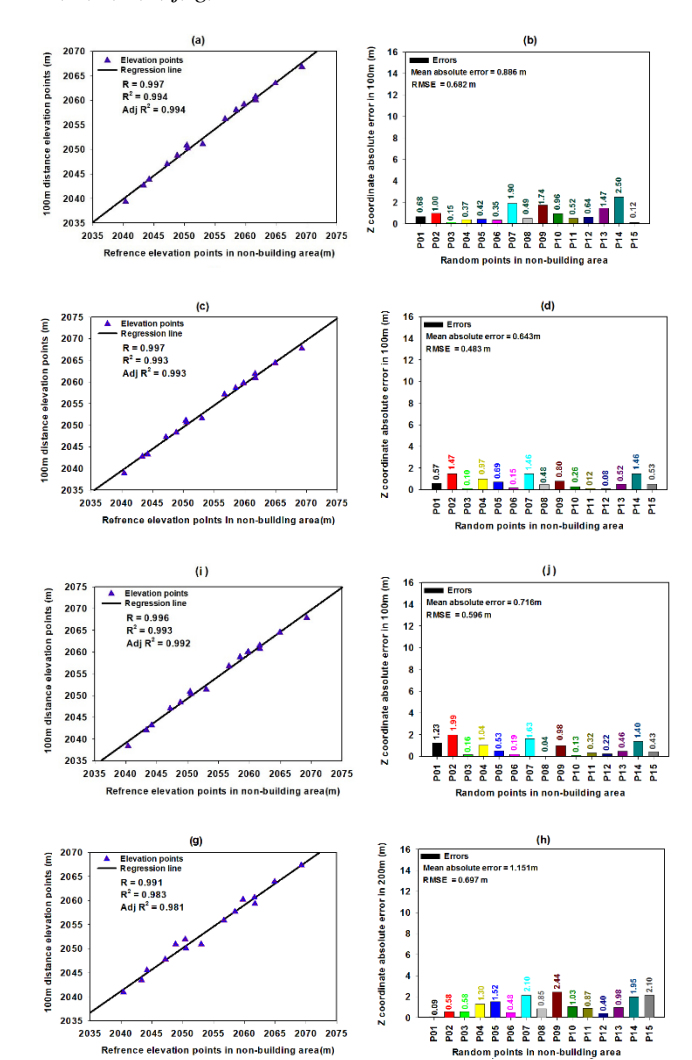
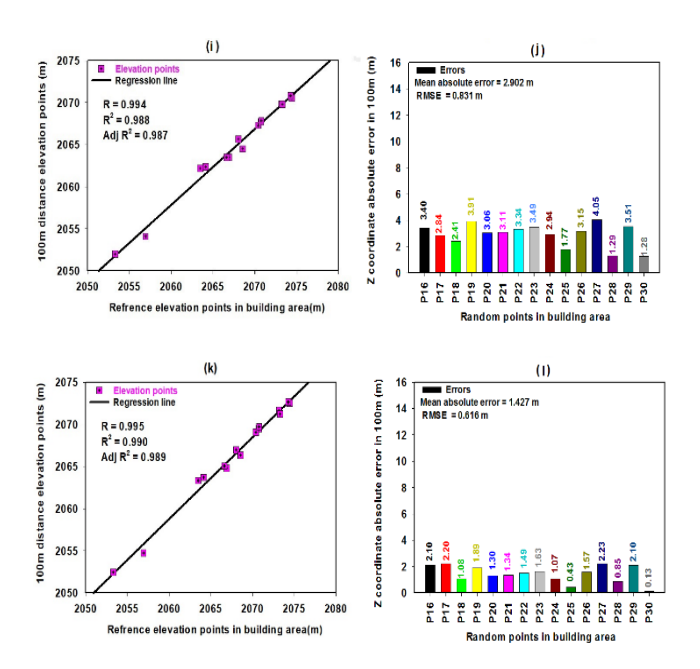


Figure 8. The regression, RMSE, and MAE values of elevation between random and reference points in the non-building region: (a and b) in mode A, (c and d) in mode B, (i and j) in mode C, and (g and h) in mode D in the first scenario

Figures 8a, b, c, d, i, j, g, and 8h demonstrate that when the distances between GCPs for the generation of UAV photogrammetry outputs are anticipated to be about 1D, modes B and D achieve the best and worst accuracy in terms of RMSE and MAE, respectively. In mode B, the GCPs were embedded in practically all of the block's side models, and there were no control points in the center of the block, but in mode D, the GCPs were only considered in the block's central models. As UAV imagery expands outside the network of GCPs, the accuracy of photogrammetry output outcomes deteriorates. Moreover, the findings demonstrate that in non-building environments, the minimal accuracy loss in photogrammetric outputs in mode B is up to 48 cm and up to 64 cm in terms of RMSE and MAE, respectively. As in the first investigation, the distance between the GCPs in the urban region was considered to be roughly 1D, and the orthomosaic product and assessment results are given in Figures 9i, j, k, l, m, n, o, and 9p.



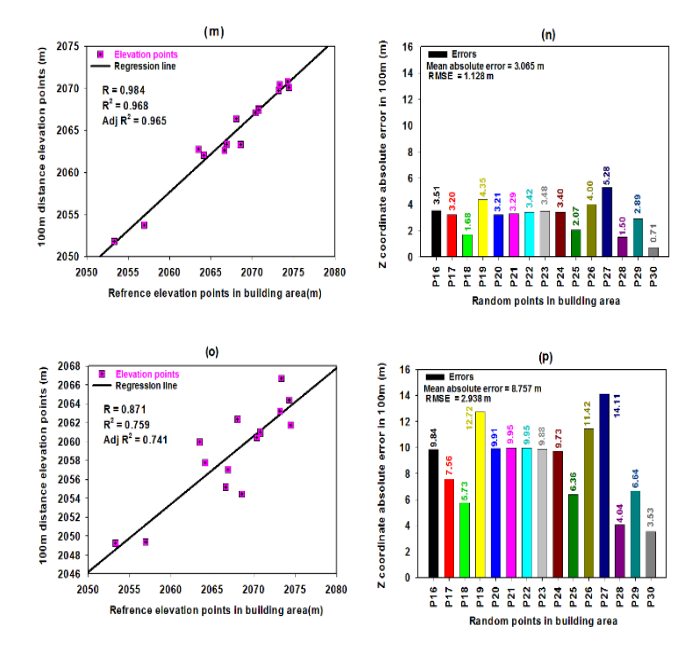


Figure 9. The regression, RMSE, and MAE values of elevation between random and reference points in the building region: (i and j) in mode A, (k and l) in mode B, (m and n) in mode C, and (o and p) in mode D in the first scenario.

Figures 9i, j, k, l, m, n, o, and 9p reveal that when the distance between the GCPs for producing UAV photogrammetric outputs is set to around 1D in building areas, modes B and D still have the best and worst accuracy in terms of RMSE and MAE, respectively. In mode B, the GCPs were effectively incorporated into all edge models of the block, and there were no control points in the center of the block, but in scenario D, the control points were only considered in the block's central models. The accuracy of photogrammetric output data degrades when UAV imagery spreads outside the network of control points.

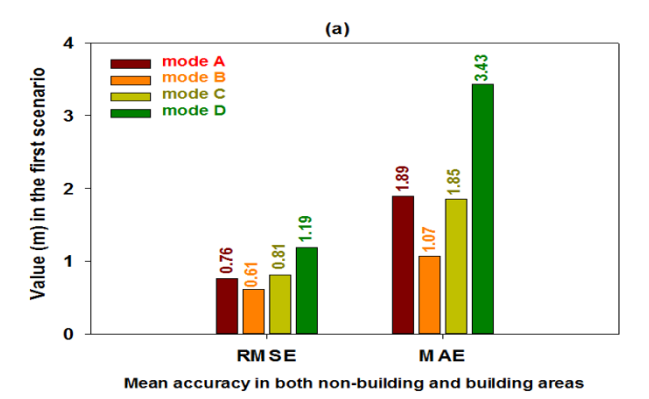


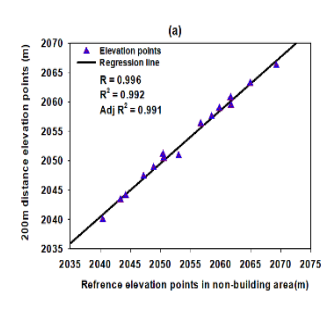
Figure 10. The UAV's photogrammetry outputs accuracy in the building and non-construction areas in the first scenario.

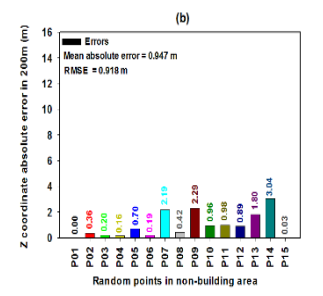
Besides that, the findings demonstrate that the minimal accuracy reduction in photogrammetric outputs in mode B in construction areas is up to 0.623 m and up to 1.43 m in terms of RMSE and MAE, respectively. Furthermore, the findings reveal that in all modes of GCP configuration patterns (A, B, C, and D) in non-building regions, the accuracy of the results in photogrammetric outputs is higher than in urban areas in terms of RMSE and MAE measures. When the average accuracy of the findings of the UAV-based photogrammetry outputs in the building and non-building areas is assessed in the first scenario, mode B yields the highest results, and mode D produces the poorest. Figure 10 illustrates the accuracy of the UAV's photogrammetry outputs in the building and non-construction areas in all four modes in the first scenario.

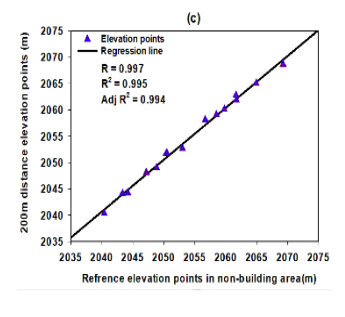
In the second scenario, the distance between the GCPs was nearly doubled, and an investigation was conducted for four modes (A, B, C, and D), and the photogrammetric output was produced again. In this scenario, the same 30 random points in both urban and non-urban regions were chosen and analyzed in the orthomosaic result for all cases. In this case, in the non-urban environment, the distance between the GCPs was deemed to be nearly twice that of the first scenario, and assessment results are shown in Figures 11 a, b, c, d, e, f, g, and 11 h.

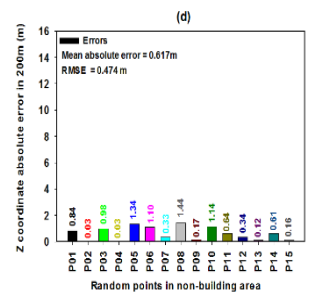
Figures 11a, b, c, d, e, f, g, and 11h demonstrate what happens when the distance between the network's GCPs is roughly doubled to provide UAV photogrammetric outputs. In this scenario, modes B and D have the highest and poorest accuracy in terms of RMSE and MAE, respectively. But nevertheless, when GCP distances double, the accuracy of UAV photogrammetry production in all modes decreases

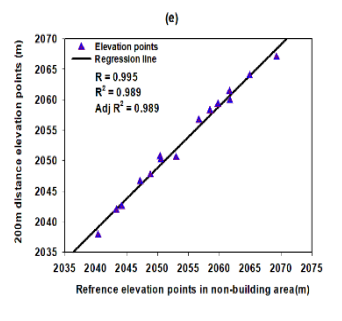
in the non-building area.

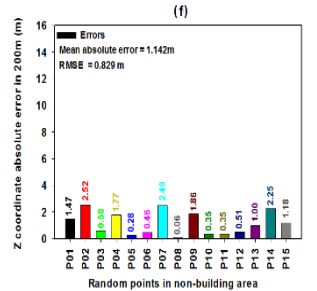


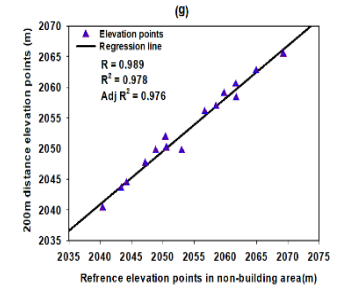












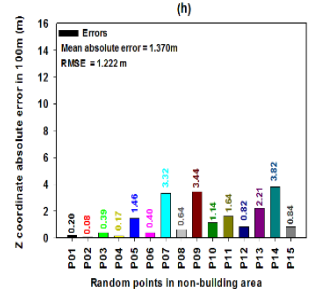
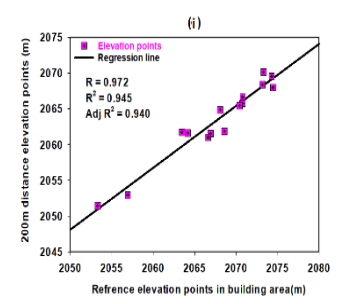
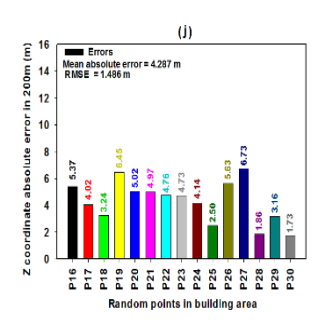


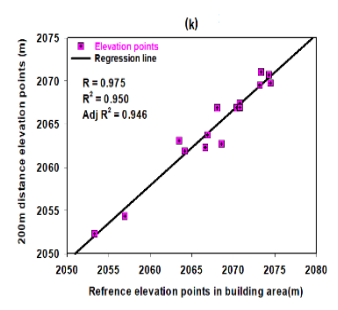
Figure 11. The regression, RMSE, and MAE values of elevation between random and reference points in the

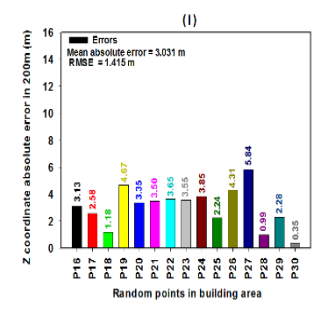
non-building region, (a and b) in mode A, (c and d) in mode B, (e and f) in mode C, and (g and h) in mode D.

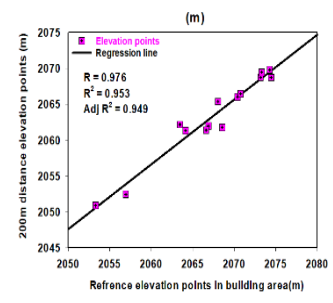
Furthermore, in the second scenario and fourth modes of investigation in the urban area, the distance between the GCPs was considered to be nearly twice that of the first scenario, and for the four modes A, B, C, and D, the evaluation results are shown in Figures 12i, j, k, l, m, n, o, and 12p.

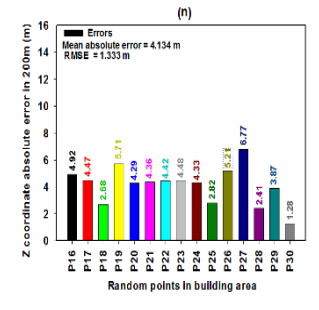


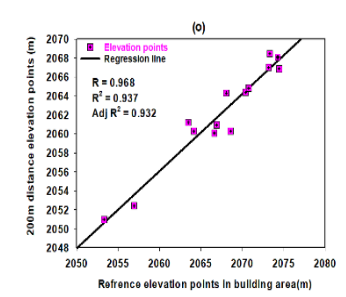












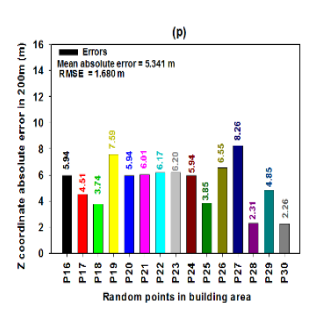
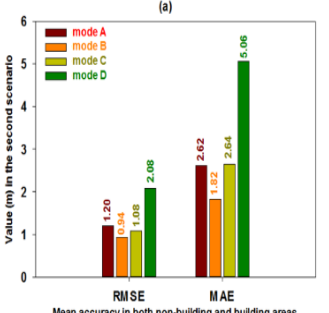


Figure 12. The regression, RMSE, and MAE values of elevation between random and reference points in the building region: (i and j) in mode A, (k and l) in mode B, (m and n) in mode C, and (o and p) in mode D in the second scenario.

As well, when GCP distances are doubled, the accuracy of UAV photogrammetry output drops in all modes in the construction area. This decrease in accuracy is obtained by increasing the distances between GCPs in the best-case B construction regions to 80 cm (1.415 m to 0.616 m) and to 1.60 m (3.031 m to 1.427 m), respectively, in terms of RMSE and MAE. In the second scenario, when the average accuracy of UAV-based photogrammetric output findings is tested in building and non-building regions, mode B delivers the best results while mode D generates the worst. In the second scenario, Figures 13a and 13b demonstrate the accuracy of UAV photogrammetric outputs in construction and non-construction regions in all four modes.



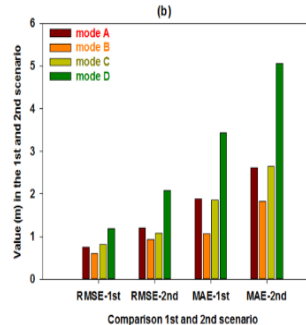


Figure 13. The accuracy of UAV photogrammetric outputs in construction and non-construction regions:
(a) mean accuracy; (b) comparison of the first and second scenarios.

In the third scenario, the distance between the GCPs was nearly tripled for modes A, B, C, and D, and the orthomosaic

output was generated again. In this scenario, the same 30 random points in both urban and non-urban regions were selected and examined in the orthomosaic output for all cases. In this scenario, in non-urban terrain, the distance between the GCPs was considered to be almost three times that of the first scenario, and assessment findings are shown in Figures 14a, b, c, d, e, f, g, and 14h.

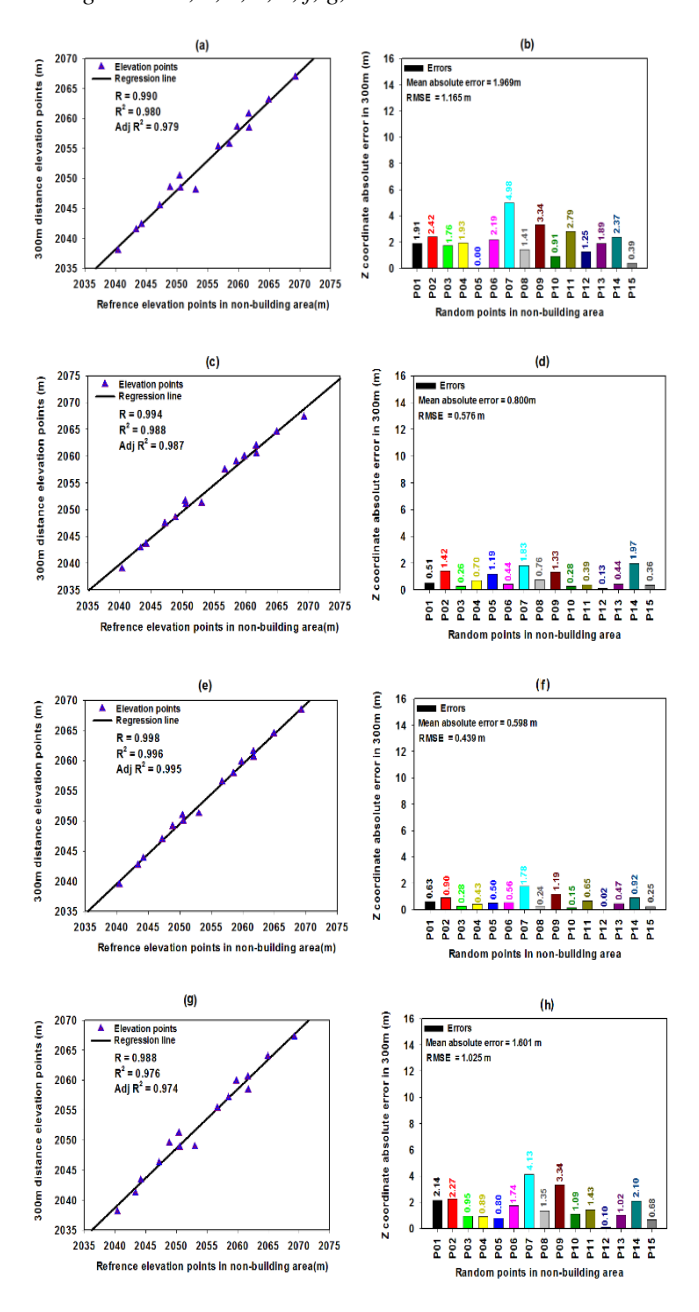
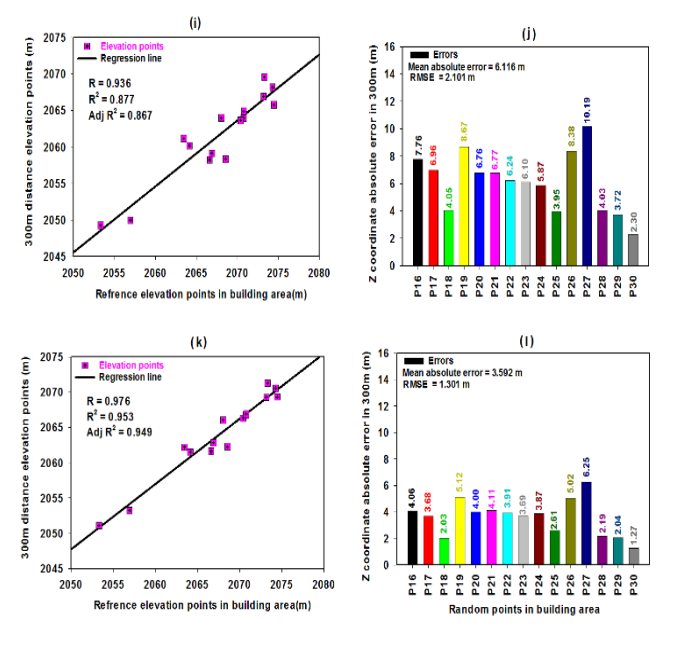
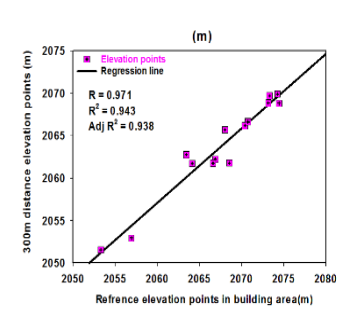


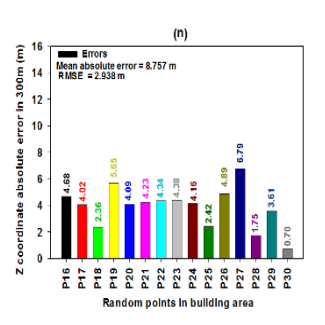
Figure 14. The regression, RMSE, and MAE values of elevation between random and reference points in the non-building region: (a and b) in mode A, (c and d) in

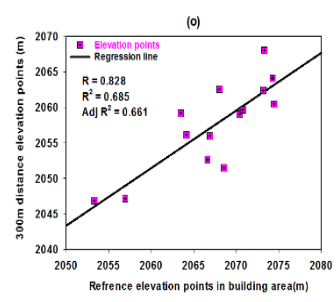
mode B, (e and f) in mode D, and (g and h) in mode D in the third scenario.

Figures 14a, b, c, d, e, f, g, and 14h demonstrate what happens when the distance between GCPs is almost tripled compared to the first scenario to obtain UAV photogrammetric outputs. In this scenario, modes B and D have the highest and lowest accuracy in terms of RMSE and MAE, respectively. When the distance between GCPs in the corner models of the photogrammetry block is tripled, better results are obtained in UAV photogrammetry finding in the non-building areas of mode C compared to mode D; that is, when the distance between control points in the corner models of the block increases, the design of GCPs in the central models of the block is required, and better results are obtained. Moreover, in the third scenario, the distance between the GCPs was considered to be almost three times greater than in the first scenario, and for the four modes A, B, C, and D, the performance evaluations are shown in Figures 15i, j, k, l, m, n, o, and 15p.









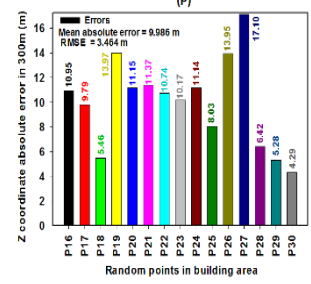
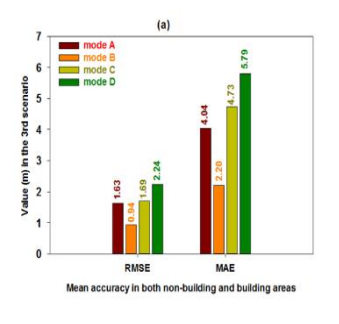


Figure 15. The regression, RMSE, and MAE values of elevation between random and reference points in the non-building region: (i and j) in mode A, (k and l) in mode B, (m and n) in mode D, and (o and p) in mode D in the third scenario.

Figures 15i, j, k, l, m, n, o, and 15p demonstrate what happens when the distance between GCPs is almost tripled compared to the first scenario to obtain UAV photogrammetric outputs in the building area. In this scenario, modes C and D have the highest and lowest accuracy in terms of RMSE and MAE, respectively. Besides this, as GCP distances are doubled and tripled, the accuracy of UAV photogrammetric output in all modes in the construction area decreases. In this scenario, mode C offers the greatest results when the average accuracy of UAVbased photogrammetric output findings is examined in builtup and unbuilt-up areas, whereas mode D generates the weakest. Figures 16a, b, and 16c in the third scenario compare the accuracy of UAV photogrammetric outputs in construction and non-construction regions in all four modes to the first and second scenarios.



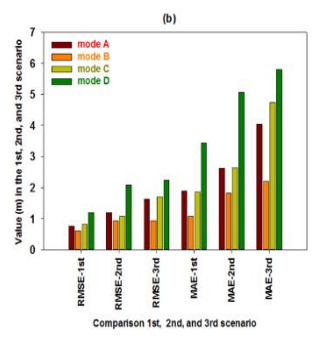


Figure 16. The accuracy of UAV photogrammetric outputs in construction and non-construction regions: (a) mean accuracy, (b) comparison of the first, second, and third scenarios.

So far, when the GCP distances are doubled and tripled, the accuracy of UAV photogrammetry output in all modes in both built-up and non-built-up areas is significantly reduced.

3.2 Multiscale model to model cloud comparison (M3C2)

In this study, the findings were evaluated both locally and globally. The results were evaluated locally using 30 random points and globally using the multiscale model-tomodel cloud comparison (M3C2) approach in both building and non-building zones. The M3C2 (multiscale model-tomodel cloud comparison) approach, developed by Lague et al. (2013), allows for direct 3D point cloud comparison by measuring distances perpendicular to local surface normals, avoiding the requirement for meshing or gridding, and showing resilience for irregular datasets. This work uses M3C2 in conjunction with UAV photogrammetry and SfM-derived models to assess surface changes and alignment accuracy while also examining statistical metrics (mean and standard deviation) of M3C2 distances. The mean distance shows systemic biases or alignment errors caused by the amount and distribution of ground control points (GCPs), whereas the standard deviation represents local variability caused by surface roughness, vegetation, or GCP mispositioning. Positive/negative mean represent vertical model displacement (new above/below reference), whereas near-zero means indicate correct alignment. A low standard deviation (σ) denotes consistent accuracy, while a large σ indicates noise, surface complexity, or mistakes. These findings are consistent with The method's integration with CloudCompare and sensitivity to GCP setups demonstrate its usefulness in assessing 3D reconstruction reliability. In this section, we explore point cloud error in general rather than analyzing it locally in the modes studied in the previous section. Recently, 3D point cloud comparison has been utilized to quantify surface changes. Two techniques have been

pursued to this end: 3D tracking of homologous regions of the surface to calculate a displacement area and distance computation between two point clouds when homologous parts cannot be specified. Lague, Brodu, Leroux, and sensing (2013) provide a multiscale model-to-model cloud comparison (M3C2) method that does a direct comparison of point clouds in 3D. This technique has three distinguishing attributes: i) it acts directly on point clouds without meshing or gridding. It computes the local distance between two point clouds along the typical surface direction, tracking 3D fluctuations in surface orientation, and it determines a confidence range for each distance measurement based on point cloud roughness and registration error.

Furthermore, when M3C2 was computed between the point clouds acquired for this research from different approaches and the reference point cloud, it proved accurate in all situations when the distance between the GCPs was doubled. Figures 18e, f, g, and 18h achieved the desired outcomes. The M3C2 method is used to calculate the orthogonal distance between two point clouds. The M3C2 additionally employs a local measure of cloud roughness and a statistical significance test for recorded changes. The M3C2 method incorporates numerous new aspects that ease the comparison of point clouds of natural settings in 3D while also allowing for the detection of extremely small surface changes and determining their statistical significance (see Figure 17).

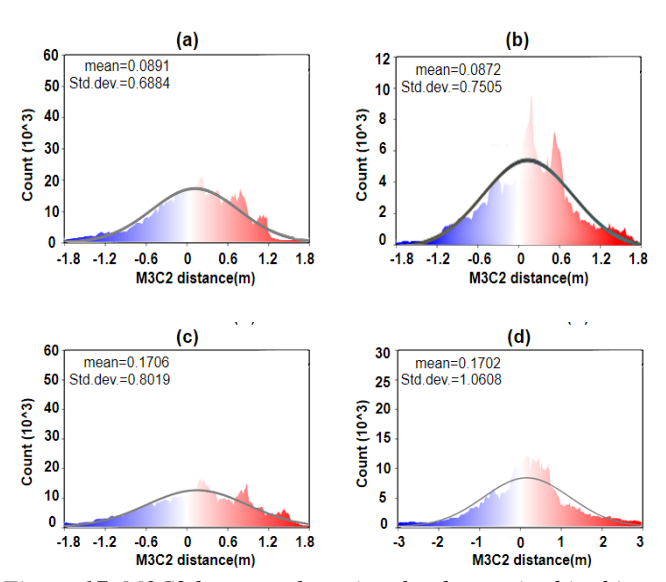


Figure 17. M3C2 between the point clouds acquired in this study from different modes and the reference point cloud, (a) mode A, (b) mode B, (c) mode C, and (d) mode D, in the first scenario.

Figures 17a, b, c, and 17d demonstrate M3C2 between the point clouds obtained in this research from various modes and the reference point cloud in (a) mode A, (b) mode B, (c) mode C, and (d) mode D, respectively, in the first scenario (1D). When all GCPs are designed around and in the central location of the photogrammetry block, Mode C has the best accuracy and the least error compared to the other three possible situations.

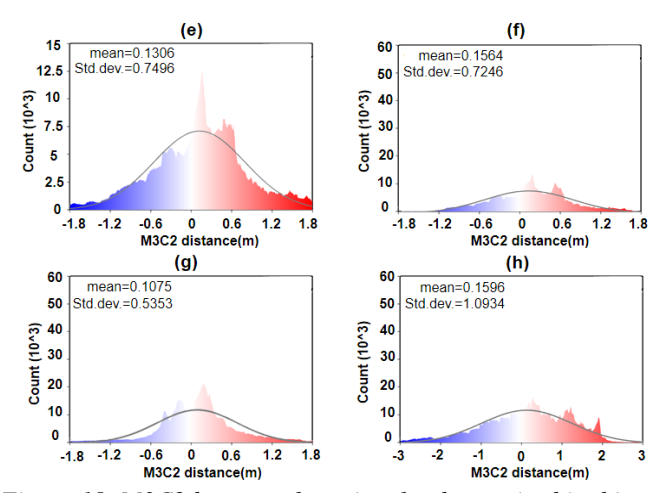
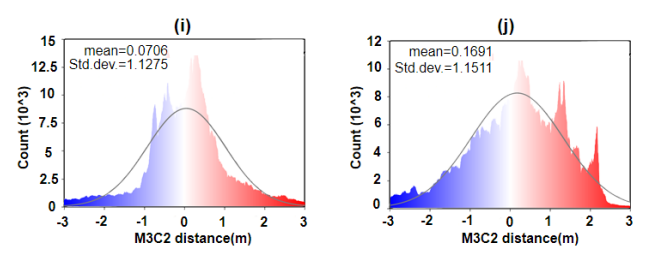
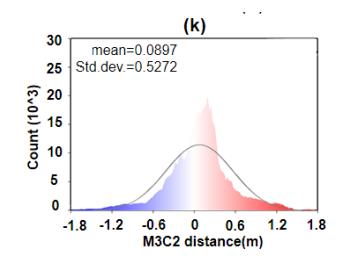


Figure 18. M3C2 between the point clouds acquired in this study from different modes and the reference point cloud: (e) mode A, (f) mode B, (g) mode C, and (h) mode D in the second scenario.

Figures 18e, f, g, and 18h demonstrate M3C2 between the point clouds (e) in mode A, (f) in mode B, (g) in mode C, and (h) in mode D, respectively, in the second scenario (2D) and the reference point cloud. When the distances between the GCPs in all modes are doubled in comparison to the first scenario, the M3C2 distance grows poorer, and the average and standard deviation come out with greater inaccuracy. Mode C, in which all GCPs are constructed around and in the center position of the photogrammetry block, likewise has higher accuracy than other modes in this scenario.





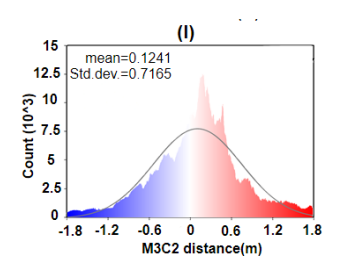


Figure 19. M3C2 between the point clouds acquired in this study from different modes and the reference point cloud, (i) mode A, (j) mode B, (k) mode C, and (l) mode D, in the third scenario.

Figures 19i, j, k, and 19l additionally generated the required outcomes when the distance between the GCPs was tripled in contrast to the first scenario. Figures 19i, j, k, and 19l show M3C2 between the point clouds (i) in mode A, (j) in mode B, (k) in mode C, and (l) in mode D in the third scenario (3D) and the reference point cloud, respectively. Again, mode C offers more accuracy than other modes in this case since all GCPs are created around and in the central location of the photogrammetry block. In addition, mode D has the lowest accuracy in all three scenarios in all modes of M3C2 investigation. Moreover, a total of three instances of comparison point clouds from the first, second, and third situations were chosen to represent the error distribution for distance M3C2 computed between reference point clouds and point clouds derived from photogrammetry products, as shown in Figures 20m, n, and 20o.

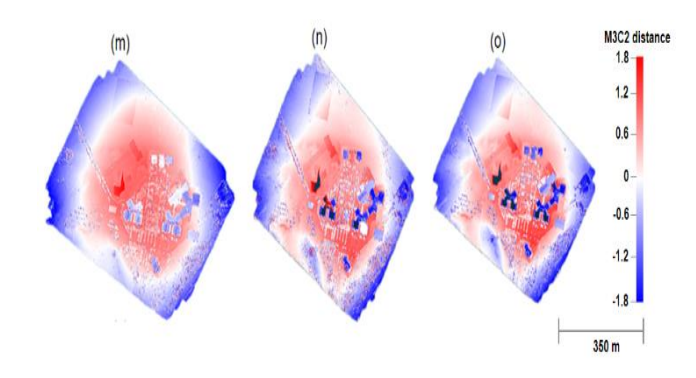


Figure 20. Error distribution for distance M3C2 computed between different modes and the reference point clouds from the first, second, and third scenarios.

The results of the error distribution for distance M3C2 in Figure 20 reveal that errors are more prevalent in the research area's border areas than in the center sections. The reason for this is that the longitudinal and side overlap of the images is frequently less extensive in border areas than

in the center parts. As a result, they have greater inaccuracy in producing cloud points than the photogrammetric block's center sections. The necessity to decrease error in the photogrammetric block's border regions is to design more control points in the block's side models, which the design modes of mode B and mode C affirm. Furthermore, in building areas with insufficient texture and a homogeneous surface, such as those in our research region, the point clouds formed do not have an appropriate density in the compromise, leading the distance from the control points to expand in these positions. If they approve it, the error will be much greater. Furthermore, the accuracy of production point clouds will be reduced in areas where topographic features vary abruptly due to the presence of structures or vegetation, such as trees.

4. Conclusions

A number of factors impact the accuracy of UAV photogrammetry results. While carefully examining the spatial distribution pattern of GCPs, as well as their quantity and optimal distance, the following two essential aims are pursued: The primary objective of this study is to assess the impact of GCP's network configuration pattern, number, and spatial distribution onUAV-based photogrammetry and 3D reconstruction accuracy. The second objective is to determine the optimal distances between the GCPs in order to improve the accuracy of the orthomosaic acquired by UAV photogrammetry. To that end, four alternative A, B, C, and D modes-in three scenarios with different GCP spatial distributions and configurations—were analyzed to determine the optimal GCP distance. Mode A was used for generating a minimum number of GCPs in the corners of the UAV photogrammetry block; mode B was used to establish GCPs in all models around the photogrammetry block; mode C was used to develop GCPs around and in the middle of the photogrammetry block; and mode D was used to set up GCPs only in the middle and center of the photogrammetry block. Furthermore, in all modes A, B, C, and D in the first scenario, the appropriate GCP distances chosen for processing the UAV photogrammetric operations and their output were approximately 1D (= 30* GSD = 100 m). The 1D distance was chosen because it is less than 30 times GSD or less than 3 times the airbase between two successive images with an average longitudinal coverage of 80%. Choosing a distance shorter than this is not cost-effective since it increases the number of GCPs necessary for UAV photogrammetry output and raises the project's cost. In addition, in the second and third scenarios, GCP distances were approximately chosen in 2D and 3D, respectively. That is, the total number of GCPs used in all modes varies from 4 to 42, depending on the distance between the GCPs. The findings were assessed locally using 30 random points in the

building and non-building regions, as well as globally using the M3C2 algorithm in the four alternative A, B, C, and D modes and three scenarios. The M3C2 method incorporates numerous new aspects that ease the comparison of point clouds of natural settings in 3D while also allowing for the detection of extremely small surface changes and determining their statistical significance. For results validation, the output of all 42 GCPs was employed as a processing reference, and the product of the orthomosaic was regarded as a reference model for all other outputs in the four A, B, C, and D mods and distinct scenarios. The RMSE and MAE were utilized as accuracy metrics in this research. The outcomes of the three distinct scenarios investigated in this research, as well as the four different A, B, C, and D modes, are given in further detail below.

In the first scenario, according to the 1D findings of the local accuracy of random points, modes B and D, achieve the best and worst accuracy in both urban and non-urban zones, respectively, in terms of RMSE and MAE measures. In mode B, the GCPs were embedded in practically all of the block's side models, and there were no control points in the center of the block, but in mode D, the GCPs were only considered in the block's central models. As UAV imagery expands outside the network of control points, the accuracy of photogrammetry output outcomes deteriorates. In this situation, the least accuracy loss in photogrammetric outputs in terms of RMSE is up to 10 cm in urban areas and up to 106 cm in non-urban areas. It should be noted that the building locations in the region under examination are almost in the center of the block, and their distances from the GCPs established in the block's side models have the greatest distance; thus, the inaccuracy in these areas is significantly larger. Furthermore, the findings reveal that in all modes of GCP spatial configuration (A, B, C, and D) in non-building regions, the accuracy of the results in photogrammetric outputs is higher than in urban areas in terms of RMSE and MAE measures. When the average accuracy of the findings of the UAV-based photogrammetry outputs in the building and non-building areas is assessed in the first 1D scenario, mode B yields the highest results, and mode D produces the poorest. In addition, in the first scenario (1D), the M3C2 method between the point clouds obtained in this research from various modes and the reference point cloud demonstrated that when all GCPs are designed around and in the central location of the photogrammetry block, Mode C has the best accuracy and the least error (0.17 m and 0.80 m, respectively) compared to the other three possible situations in terms of mean errors and RMSE.

In the second scenario, the distance between the GCPs

was roughly doubled, four modes (A, B, C, and D) were investigated, and the photometric result was generated once again. In this situation, the same 30 random points were chosen and evaluated in both urban and non-urban areas. In this scenario, mode B has the highest accuracy in terms of RMSE and MAE measures. Nonetheless, when GCP distances double in the non-building region, the accuracy of UAV photogrammetry output in all modes falls. Furthermore, the distance between the GCPs in the second and fourth modes of study in the metropolitan area was assessed to be approximately double that of the first scenario and for the four modes A. B. C. and D. As well. when GCP distances are doubled, the accuracy of UAV photogrammetry output drops in all modes in the construction area. This decrease in accuracy is obtained by increasing the distances between control points in the bestmode B construction regions to 80 cm (1.415 m to 0.616 m) and to 1.60 m (3.031 m to 1.427 m), respectively, in terms of RMSE and MAE. In the second 2D scenario, when the average accuracy of UAV-based photogrammetric output findings is tested in building and non-building regions, mode B delivers the best results while mode D generates the worst. In addition, the findings of the M3C2 method in the second scenario demonstrate that when the distances between the GCPs in all modes are doubled in comparison to the first scenario, the M3C2 distance grows poorer, and the average and standard deviation come out with greater inaccuracy. Mode C, in which all control points are constructed around and in the center position of the photogrammetry block, likewise has higher accuracy than other modes in this scenario.

In the third scenario, the distance between the GCPs was nearly tripled for modes A, B, C, and D, and the photogrammetric output was generated again. In this scenario, the same random points in both urban and nonurban regions were selected and examined in the orthomosaic output for all cases. In this scenario, modes C and D have the highest and lowest accuracy in terms of RMSE and MAE, respectively. When the distance between GCPs in the corner models of the photogrammetry block is tripled, better results are obtained in UAV photogrammetry finding in the non-building areas of mode C compared to mode B; that is, when the distance between GCPs in the corner models of the block increases, the design of GCPs patterns in the central models of the block is required, and better results are obtained. Furthermore, when the GCP distances are doubled and tripled in the second and third scenarios, the accuracy of UAV photogrammetry output in all modes in both built-up and non-built-up areas is significantly reduced. As a consequence of the research, the GCP design in mode C has the lowest error of all options,

and expanding GCP intervals beyond 30 times the GSD is not recommended in the UAV geomatics projects, although when GCP distances are chosen greater than 90 GSD, the design of the GCP pattern in the central models of the block is required and better results are obtained. In addition, the findings of the globally accurate assessment utilizing the M3C2 approach revealed that mode C, when GCPs are designed around the corner and central location of the photogrammetry block, had the best outcomes and the least error in the three scenarios examined. The results of the error distribution for distance M3C2 reveal that errors are more prevalent in the research area's border areas than in the center sections.

Declaration

Conflicts of interest/Competing interests

The authors state that they do not have any competing interests.

Availability of data and material

The datasets used during the current investigation are accessible upon reasonable request from the corresponding author.

Authors' contributions

The following authors affirm their contributions to the paper: H.Emami conceived and designed the study; M.Dorzadeh collected the data; H.E. and M.D. analyzed and interpreted the results; and H.E. prepared the draft paper. The results were evaluated by all authors, and the final version of the paper was approved by all of them.

References

- Agüera-Vega, F., Carvajal-Ramírez, F., & Martínez-Carricondo, P. J. M. (2017). Assessment of photogrammetric mapping accuracy based on variation ground control points number using unmanned aerial vehicle. 98, 221-227. https://doi.org/10.1016/j.measurement.2016.12.002.
- Awasthi, B., Karki, S., Regmi, P., Dhami, D. S., Thapa, S., & Panday, U. S. (2019). Analyzing the Effect of Distribution Pattern and Number of GCPs on Overall Accuracy of UAV Photogrammetric Results. Paper presented at the International Conference on Unmanned Aerial System in Geomatics. https://doi.org/10.1007/978-3-030-37393-1_29.
- Carvajal-Ramírez, F., Agüera-Vega, F., & Martínez-Carricondo, P. J. J. o. A. R. S. (2016). Effects of image orientation and ground control points distribution on unmanned aerial vehicle

- photogrammetry projects on a road cut slope. 10(3), 034004.
- Clapuyt, F., Vanacker, V., & Van Oost, K. J. G. (2016).

 Reproducibility of UAV-based earth topography reconstructions based on Structure-from-Motion algorithms. 260, 4-15. https://doi.org/10.1016/j.geomorph.2015.05.011.
- Elkhrachy, I. J. A. E. J. (2021). Accuracy assessment of lowcost Unmanned Aerial Vehicle (UAV) photogrammetry. 60(6), 5579-5590. https://doi.org/ 10.1016/j.aej.2021.04.011.
- Erenoglu, R. C., Erenoglu, O., & Arslan, N. (2018).

 Accuracy assessment of low cost UAV based city modelling for urban planning. Tehnički vjesnik, 25(6), 1708-1714. https://doi.org/ 10.17559/TV-20170904202055.
- Fernandez Galarreta, J., Kerle, N., & Gerke, M. (2015). UAV-based urban structural damage assessment using object-based image analysis and semantic reasoning. Natural hazards and earth system sciences, 15(6), 1087-1101. https://doi.org/10.5194/nhess-15-1087-2015.
- Gindraux, S. (2019). The potential of UAV photogrammetry for hydro-glaciological forecasts. VAW-Mitteilungen, 252. https://doi.org/10.3929/ethz-b-000480081.
- James, M. R., Robson, S., d'Oleire-Oltmanns, S., & Niethammer, U. J. G. (2017). Optimising UAV topographic surveys processed with structure-frommotion: Ground control quality, quantity and bundle adjustment. 280, 51-66. https://doi.org/10.1016/j.geomorph.2016.11.021.
- Jenal, A., Lussem, U., Bolten, A., Gnyp, M. L., Schellberg, J., Jasper, J., . . . Bareth, G. (2020). Investigating the potential of a newly developed UAV-based VNIR/SWIR imaging system for forage mass monitoring. PFG—Journal of Photogrammetry, Remote Sensing and Geoinformation Science, 88(6), 493-507. https://doi.org/10.1007/s41064-020-00128-7.
- Koeva, M., Muneza, M., Gevaert, C., Gerke, M., & Nex, F. (2018). Using UAVs for map creation and updating. A case study in Rwanda. Survey Review, 50(361), 312-325. https://doi.org/10.1080/00396265.2016.1268756.
- Lague, D., Brodu, N., Leroux, J. J. I. j. o. p., & sensing, r. (2013). Accurate 3D comparison of complex topography with terrestrial laser scanner: Application to the Rangitikei canyon (NZ). 82, 10-26. https://doi.org/10.1016/j.isprsjprs.2013.04.009.
- Lalak, M., Wierzbicki, D., & Kędzierski, M. J. R. s. (2020). Methodology of processing single-strip blocks of imagery with reduction and optimization number of ground control points in UAV photogrammetry. 12(20), 3336. https://doi.org/10.3390/rs12203336.

- Liu, X., Lian, X., Yang, W., Wang, F., Han, Y., & Zhang, Y. J. D. (2022). Accuracy assessment of a UAV direct georeferencing method and impact of the configuration of ground control points. 6(2), 30. https://doi.org/10.3390/drones6020030.
- Long, N. Q., Goyal, R., Bui, L. K., Cuong, C. X., Canh, L. V., Minh, N. Q., & Bui, X. N. J. A. o. M. S. (2021). Optimal choice of the number of ground control points for developing precise DSM using light-weight UAV in small and medium-sized open-pit mine. 66(3). https://doi.org/10.24425/ams.2021.138594.
- Martínez-Carricondo, P., Agüera-Vega, F., Carvajal-Ramírez, F., Mesas-Carrascosa, F.-J., García-Ferrer, A., Pérez-Porras, F.-J. J. I. j. o. a. e. o., & geoinformation. (2018). Assessment of UAV-photogrammetric mapping accuracy based on variation of ground control points. 72, 1-10. https://doi.org/10.1016/j.jag.2018.05.015.
- Nagendran, S. K., Tung, W. Y., & Ismail, M. A. M. (2018).

 Accuracy assessment on low altitude UAV-borne photogrammetry outputs influenced by ground control point at different altitude. Paper presented at the IOP Conference Series: Earth and Environmental Science. https://doi.org/10.1088/1755-1315/169/1/012031.
- Nex, F., Armenakis, C., Cramer, M., Cucci, D. A., Gerke, M., Honkavaara, E., . . . Skaloud, J. (2022). UAV in the advent of the twenties: Where we stand and what is next. ISPRS journal of photogrammetry and remote sensing, 184, 215-242. https://doi.org/10.1016/j.isprsjprs.2021.12.006.
- Oniga, V.-E., Breaban, A.-I., Pfeifer, N., & Chirila, C. J. R. S. (2020). Determining the suitable number of ground control points for UAS images georeferencing by varying number and spatial distribution. 12(5), 876. https://doi.org/10.3390/rs12050876.
- Peppa, M. V., Mills, J. P., Moore, P., Miller, P. E., & Chambers, J. E. (2019). Automated co registration and calibration in SfM photogrammetry for landslide change detection. Earth Surface Processes and Landforms, 44(1), 287-303. https://doi.org/10.1002/esp.4502.
- Reshetyuk, Y., & Mårtensson, S. G. J. T. P. R. (2016). Generation of highly accurate digital elevation models with unmanned aerial vehicles. 31(154), 143-165.

- https://doi.org/10.1111/phor.12143.
- Sanz-Ablanedo, E., Chandler, J. H., Rodríguez-Pérez, J. R., & Ordóñez, C. (2018). Accuracy of unmanned aerial vehicle (UAV) and SfM photogrammetry survey as a function of the number and location of ground control points used. Remote Sensing, 10(10), 1606. d https://doi.org/10.3390/rs10101606.
- Stöcker, C., Nex, F., Koeva, M., & Gerke, M. J. R. s. (2020). High-quality uav-based orthophotos for cadastral mapping: Guidance for optimal flight configurations. 12(21), 3625. https://doi.org/10.3390/rs12213625.
- Tu, Y.-H., Phinn, S., Johansen, K., Robson, A., Wu, D. J. I. J. o. P., & Sensing, R. (2020). Optimising drone flight planning for measuring horticultural tree crop structure. 160, 83-96. https://doi.org/10.1016/j.isprsjprs.2019.12.006.
- Varbla, S., Puust, R., & Ellmann, A. J. S. r. (2021). Accuracy assessment of RTK-GNSS equipped UAV conducted as-built surveys for construction site modelling. 53(381), 477-492. https://doi.org/10.1080/00396265.2020.1830544.
- Villanueva, J., Blanco, A. J. T. I. A. o. P., Remote Sensing, & Sciences, S. I. (2019). Optimization of ground control point (GCP) configuration for unmanned aerial vehicle (UAV) survey using structure from motion (SFM). 42, 167-174. https://doi.org/ 10.5194/isprs-archives-XLII-4-W12-167-2019.
- Yin, H., Huang, W., Li, F., Yang, H., Li, Y., Hu, Y., & Yu, K. (2023). Multi-temporal UAV Imaging-Based Mapping of Chlorophyll Content in Potato Crop. PFG—Journal of Photogrammetry, Remote Sensing and Geoinformation Science, 91(2), 91-106. https://doi.org/10.1007/s41064-022-00218-8.
- Zhang, K., Okazawa, H., Hayashi, K., Hayashi, T., Fiwa, L., & Maskey, S. J. S. (2022). Optimization of Ground Control Point Distribution for Unmanned Aerial Vehicle Photogrammetry for Inaccessible Fields. 14(15), 9505. https://doi.org/10.3390/su14159505.